Monte Carlo determination of the low-energy constants of a spin-$\frac{1}{2}$ Heisenberg model with spatial anisotropy

F.-J. Jiang,[1,*] F. Kämpfer,[2] and M. Nyfeler[1]

[1]*Center for Research and Education in Fundamental Physics, Institute for Theoretical Physics, Bern University, Sidlerstrasse 5, CH-3012 Bern, Switzerland*

[2]*Department of Physics, Condensed Matter Theory Group, Massachusetts Institute of Technology (MIT), 77 Massachusetts Avenue, Cambridge, Massachusetts 02139, USA*

(Received 6 March 2009; revised manuscript received 15 May 2009; published 14 July 2009)

Motivated by the possible mechanism for the pinning of the electronic liquid crystal direction in $YBa_2Cu_3O_{6.45}$ as proposed by Pardini *et al.* [Phys. Rev. B **78**, 024439 (2008)], we use the first-principles Monte Carlo method to study the spin-$\frac{1}{2}$ Heisenberg model with antiferromagnetic couplings J_1 and J_2 on the square lattice. In particular, the low-energy constants spin stiffness ρ_s, staggered magnetization $\mathcal{M}_s$, and spin wave velocity c are determined by fitting the Monte Carlo data to the predictions of magnon chiral perturbation theory. Further, the spin stiffnesses ρ_{s1} and ρ_{s2} as a function of the ratio J_2/J_1 of the couplings are investigated in detail. Although we find a good agreement between our results with those obtained by the series expansion method in the weakly anisotropic regime, for strong anisotropy we observe discrepancies.

DOI: 10.1103/PhysRevB.80.033104 PACS number(s): 12.39.Fe, 75.10.Jm, 75.40.Mg, 75.50.Ee

I. INTRODUCTION

Understanding the mechanism responsible for high-temperature superconductivity in cuprate materials remains one of the most active research fields in condensed-matter physics. Unfortunately, the theoretical understanding of the high-T_c materials using analytic methods as well as first-principles Monte Carlo simulations is hindered by the strong electron correlations in these materials. Despite this difficulty, much effort has been devoted to investigating the properties of the relevant t-J-type models for the high-T_c cuprates.[1–4] Although a conclusive agreement regarding the mechanism responsible for the high-T_c phenomena has not been reached yet, it is known that the high-T_c cuprate superconductors are obtained by doping the antiferromagnetic insulators with charge carriers. This has triggered vigorous studies of undoped and lightly doped antiferromagnets. Today, the undoped antiferromagnets on the square lattice such as La_2CuO_4 are among the quantitatively best understood condensed-matter systems.

Spatially anisotropic Heisenberg models have been studied intensely due to their phenomenological importance as well as from the perspective of theoretical interest.[5–8] For example, numerical evidence indicates that the anisotropic Heisenberg model with staggered arrangement of the antiferromagnetic couplings may belong to a new universality class, in contradiction to the $O(3)$ universality predictions.[9] Further, it is argued that the Heisenberg model with spatially anisotropic couplings J_1 and J_2, as depicted in Fig. 1, is relevant to the newly discovered pinning effects of the electronic liquid crystal in the underdoped cuprate superconductor $YBa_2Cu_3O_{6.45}$.[10,11] It is observed that the $YBa_2Cu_3O_{6.45}$ compound has a tiny in-plane lattice anisotropy which is strong enough to pin the orientation of the electronic liquid crystal in a particular direction. The authors of Ref. 12 demonstrated that the in-plane anisotropy of the spin stiffness of the Heisenberg model with spatially anisotropic couplings J_1 and J_2 can provide a possible mechanism for the pinning of the electronic liquid crystal direction in $YBa_2Cu_3O_{6.45}$.

Since the anisotropy of the spin stiffness in the spin-$\frac{1}{2}$ Heisenberg model with different antiferromagnetic couplings J_1 and J_2 has not been studied in detail before with first-principles Monte Carlo methods, in this Brief Report we perform a Monte Carlo calculation to determine the low-energy constants, namely, the spin stiffnesses ρ_{s1} and ρ_{s2}, staggered magnetization $\mathcal{M}_s$, and spin wave velocity c. In particular, we investigate the J_2/J_1 dependence of ρ_{s1} and ρ_{s2}, and find good agreement with earlier studies[12] using series expansion methods in the weakly anisotropic regime. Our finding would lead to very strong pinning energy per Cu site in $YBa_2Cu_3O_{6.45}$ as claimed in Ref. 12. However, deviations appear as one moves toward strong anisotropy. We argue that the deviations observed between our results and the naive expectation might indicate an unexpected behavior of the spin stiffness ρ_s at extremely strong anisotropy.

II. MICROSCOPIC MODELS AND CORRESPONDING OBSERVABLES

The Heisenberg model we consider in this study is defined by the Hamilton operator

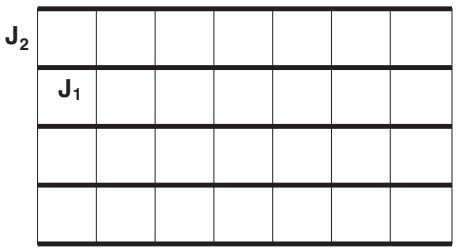

FIG. 1. The anisotropic Heisenberg model investigated in this study. J_1 and J_2 are the antiferromagnetic couplings in the 1- and 2-directions, respectively.

$$H = \sum_x [J_1 \vec{S}_x \cdot \vec{S}_{x+\hat{1}} + J_2 \vec{S}_x \cdot \vec{S}_{x+\hat{2}}], \quad (1)$$

where $\hat{1}$ and $\hat{2}$ refer to the two spatial unit vectors. Further, J_1 and J_2 in Eq. (1) are the antiferromagnetic couplings in the 1- and 2-directions, respectively. A physical quantity of central interest is the staggered susceptibility (corresponding to the third component of the staggered magnetization M_s^3) that is given by

$$\chi_s = \frac{1}{L_1 L_2} \int_0^\beta dt \frac{1}{Z} \mathrm{Tr}[M_s^3(0) M_s^3(t) \exp(-\beta H)]. \quad (2)$$

Here β is the inverse temperature, L_1 and L_2 are the spatial box sizes in the one and two directions, respectively, and $Z = \mathrm{Tr}\exp(-\beta H)$ is the partition function. The staggered magnetization order parameter $\vec{M}_s$ is defined as $\vec{M}_s = \Sigma_x (-1)^{x_1+x_2} \vec{S}_x$. Another relevant quantity is the uniform susceptibility that is given by

$$\chi_u = \frac{1}{L_1 L_2} \int_0^\beta dt \frac{1}{Z} \mathrm{Tr}[M^3(0) M^3(t) \exp(-\beta H)]. \quad (3)$$

Here $\vec{M} = \Sigma_x \vec{S}_x$ is the uniform magnetization. Both χ_s and χ_u can be measured very efficiently with the loop-cluster algorithm using improved estimators.[13] In particular, in the multicluster version of the algorithm the staggered susceptibility is given in terms of the cluster sizes $|\mathcal{C}|$ (which have the dimension of time), i.e., $\chi_s = \frac{1}{\beta L_1 L_2} \langle \Sigma_{\mathcal{C}} |\mathcal{C}|^2 \rangle$. Similarly, the uniform susceptibility $\chi_u = \frac{\beta}{L_1 L_2} \langle W_t^2 \rangle = \frac{\beta}{L_1 L_2} \langle \Sigma_{\mathcal{C}} W_t(\mathcal{C})^2 \rangle$ is given in terms of the temporal winding number $W_t = \Sigma_{\mathcal{C}} W_t(\mathcal{C})$, which is the sum of winding numbers $W_t(\mathcal{C})$ of the loop clusters $\mathcal{C}$ around the Euclidean time direction. Similarly, the spatial winding numbers are defined by $W_i = \Sigma_{\mathcal{C}} W_i(\mathcal{C})$ with $i \in \{1,2\}$.

III. LOW-ENERGY EFFECTIVE THEORY FOR MAGNONS

Due to the spontaneous breaking of the $SU(2)_s$ spin symmetry down to its $U(1)_s$ subgroup, the low-energy physics of antiferromagnets is governed by two massless Goldstone bosons, the antiferromagnetic spin waves or magnons. The description of the low-energy magnon physics by an effective theory was pioneered by Chakravarty *et al.*[14] A systematic low-energy effective field theory for magnons was further developed in Refs. 15–17. The staggered magnetization of an antiferromagnet is described by a unit-vector field $\vec{e}(x)$ in the coset space $SU(2)_s/U(1)_s = S^2$, i.e., $\vec{e}(x) = [e_1(x), e_2(x), e_3(x)]$ with $\vec{e}(x)^2 = 1$. Here $x = (x_1, x_2, t)$ denotes a point in $(2+1)$-dimensional space-time. To leading order, the Euclidean magnon low-energy effective action takes the form

$$S[\vec{e}] = \int_0^{L_1} dx_1 \int_0^{L_2} dx_2 \int_0^\beta dt \times \left(\frac{\rho_{s1}}{2} \partial_1 \vec{e} \cdot \partial_1 \vec{e} + \frac{\rho_{s2}}{2} \partial_2 \vec{e} \cdot \partial_2 \vec{e} + \frac{\rho_s}{2c^2} \partial_t \vec{e} \cdot \partial_t \vec{e} \right), \quad (4)$$

where the index $i \in \{1,2\}$ labels the two spatial directions and t refers to the Euclidean time direction. The parameters $\rho_s = \sqrt{\rho_{s1} \rho_{s2}}$, ρ_{s1}, and ρ_{s2} are the spin stiffness in the temporal and spatial directions, respectively, and c is the spin wave velocity. Rescaling $x_1' = (\rho_{s2}/\rho_{s1})^{1/4} x_1$ and $x_2' = (\rho_{s1}/\rho_{s2})^{1/4} x_2$, Eq. (4) can be rewritten as

$$S[\vec{e}] = \int_0^{L_1'} dx_1' \int_0^{L_2'} dx_2' \int_0^\beta dt \frac{\rho_s}{2} \left(\partial_i' \vec{e} \cdot \partial_i' \vec{e} + \frac{1}{c^2} \partial_t \vec{e} \cdot \partial_t \vec{e} \right). \quad (5)$$

Additionally requiring $L_1' = L_2' = L$ we obey the condition of square area. Notice that the effective field theories described by Eqs. (4) and (5) are valid as long as the conditions $L_i \beta \rho_{s1} \gg 1$ and $L_i \beta \rho_{s2} \gg 1$ for $i \in \{1,2\}$ hold, which is indeed the case for the setup of this study. Once these conditions are satisfied, the low-energy physics of the underlying microscopic model can be captured quantitatively by the effective field theory as demonstrated in Ref. 13. Further, in the so-called cubical regime (to be defined later), which is relevant to our study, the cutoff effects appear in the free-energy density only at next-to-next-to-next-to-leading order (NNNLO). The finite cutoff leads to higher-order terms in the effective Lagrangian due to the breaking of some symmetries and it introduces the cutoff dependence in the Fourier integrals (sums). By employing similar arguments as those presented in Ref. 18, one can show that higher-order corrections to Eq. (4) contain four derivatives and the leading cutoff effect in the Fourier integrals (sums) enters the free-energy density only at NNNLO. Therefore Eq. (5) is sufficient to derive up to next-to-next-to-leading order (NNLO) contributions to the observables considered here. We have further verified that the inclusion of NNNLO contributions to the relevant observables considered here lead to statistically consistent results with those not taking such corrections into account. Hence the volume and temperature dependences of χ_s and χ_u up to NNLO (to be presented below) are sufficient to describe our numerical data quantitatively, and the finite cutoff effects are negligible. Using above Euclidean action (5), detailed calculations of a variety of physical quantities including the NNLO contributions have been carried out in Ref. 18. Here we only quote the results that are relevant to our study, namely, the finite-temperature and finite-volume effects of the staggered susceptibility and the uniform susceptibility. The aspect ratio of a spatially quadratic space-time box with box size L is characterized by $l = (\beta c/L)^{1/3}$, with which one distinguishes cubical space-time volumes with $\beta c \approx L$ from cylindrical ones with $\beta c \gg L$. In the cubical regime, the volume and temperature dependences of the staggered susceptibility is given by

$$\chi_s = \frac{\mathcal{M}_s^2 L^2 \beta}{3} \left\{ 1 + 2 \frac{c}{\rho_s L l} \beta_1(l) + \left(\frac{c}{\rho_s L l} \right)^2 [\beta_1(l)^2 + 3\beta_2(l)] + O\left(\frac{1}{L^3} \right) \right\}, \quad (6)$$

where $\mathcal{M}_s$ is the staggered magnetization density. Finally the uniform susceptibility takes the form

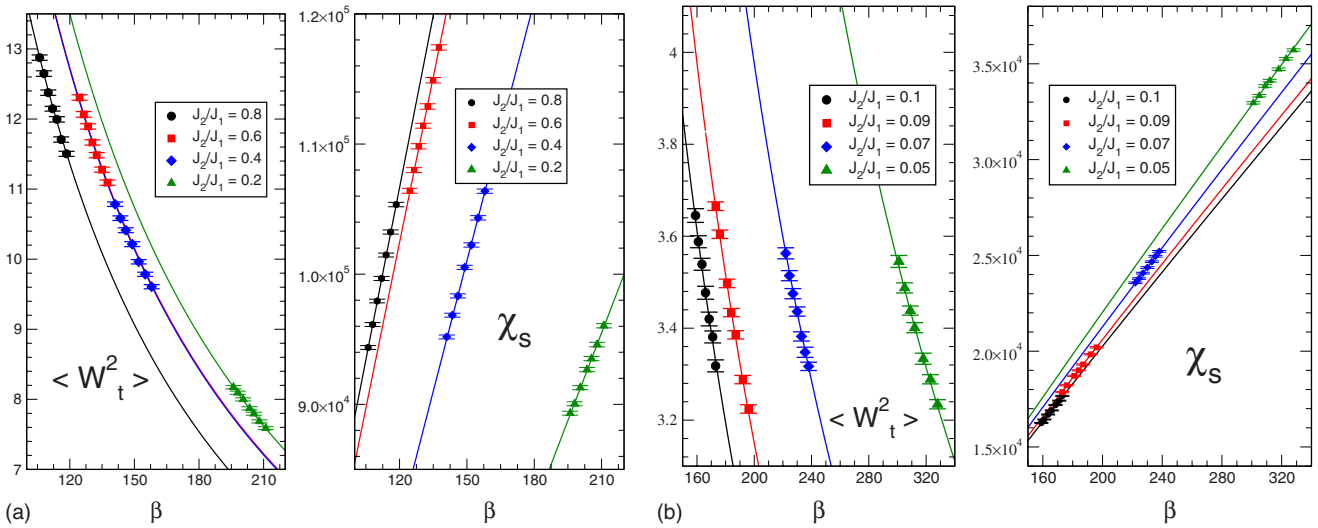

FIG. 2. (Color online) Comparison between our numerical results (data points) and the theoretical predictions (solid lines) that are obtained by using the low-energy parameters from the fits.

$$\chi_u = \frac{2\rho_s}{3c^2}\left\{1 + \frac{1}{3}\frac{c}{\rho_s L l}\tilde{\beta}_1(l) + \frac{1}{3}\left(\frac{c}{\rho_s L l}\right)^2 \times\left[\tilde{\beta}_2(l) - \frac{1}{3}\tilde{\beta}_1(l)^2 - 6\psi(l)\right] + O\left(\frac{1}{L^3}\right)\right\}. \quad (7)$$

In Eqs. (6) and (7), the functions $\beta_i(l)$, $\tilde{\beta}_i(l)$, and $\psi(l)$, which only depend on l, are shape coefficients of the space-time box defined in Ref. 18.

IV. DETERMINATION OF THE LOW-ENERGY PARAMETERS AND DISCUSSIONS

In order to determine the low-energy constants for the anisotropic Heisenberg model given in Eq. (1), we have performed simulations within the range $0.05 \leq J_2/J_1 \leq 1.0$. The cubical regime is determined by the condition $\langle \Sigma_C W_1(C)^2 \rangle \approx \langle \Sigma_C W_2(C)^2 \rangle \approx \langle \Sigma_C W_t(C)^2 \rangle$ (which implies $\beta c \approx L$). Notice that since $J_2 \leq J_1$ in our simulations, one must increase the lattice size L_1 in order to fulfill the condition $\langle \Sigma_C W_1(C)^2 \rangle = \langle \Sigma_C W_2(C)^2 \rangle$ because Eqs. (6) and (7) are obtained for a (2+1)-dimensional box with equal extent in the two spatial directions. Therefore, an interpolation of the data points is required in order to be able to use Eqs. (6) and (7). Further, the low-energy parameters are extracted by fitting the Monte Carlo data to the effective field theory predictions. The quality of these fits is good as can be seen from Fig. 2 (the χ^2/d.o.f. for all the fits is less than 1.25). Figure 3 shows ρ_{s1} and ρ_{s2}, obtained from the fits, as functions of the ratio of the antiferromagnetic couplings, J_2/J_1. The values of $\rho_{s1}(\rho_{s2})$ obtained here agree quantitatively with those obtained using the series expansion in Ref. 12 at $J_2/J_1=0.8$ and 0.6 (0.8, 0.6, 0.4, and 0.2). At $J_2/J_1=0.4$, the value we obtained for ρ_{s1} is only slightly below the corresponding series expansion result in Ref. 12. However, sizable deviations begin to show up for stronger anisotropies. Further, we have not observed the saturation of ρ_{s1} to a one-dimensional (1D) limit, namely, $0.25J_1$ as suggested in Ref. 12, even at J_2/J_1 as small as 0.05. In particular, ρ_{s1} decreases slightly as one moves from $J_2/J_1=0.1$ to $J_2/J_1=0.05$ although they still agree within statistical errors. Of course, one cannot rule out that the anisotropies in J_2/J_1 considered here are still too far away from the regime where this particular Heisenberg model can be effectively described by its 1D limit. On the other hand, the Heisenberg model considered here and its 1D limit are two completely different systems because spontaneous symmetry breaking appears only in two dimension, still $\xi=\infty$ in both cases. Further, the low-temperature behavior of χ_u in the 1D system is known to be completely different from that of the two-dimensional system.[18,19] Although intuitively one might expect a continuous transition of ρ_{s1}, one cannot rule out an unexpected behavior of ρ_{s1} as one moves from this Heisenberg model toward its 1D limit. In particular, since earlier studies indicate that long-range order already sets in even for infinitesimally small J_2/J_1,[6,20,21] it would be inter-

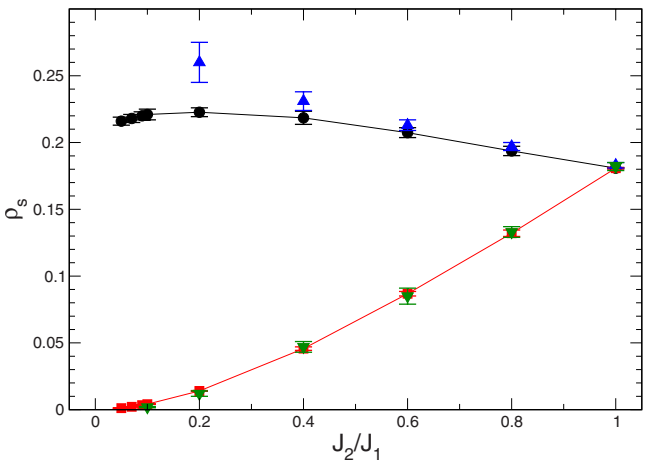

FIG. 3. (Color online) The J_2/J_1 dependence of the spin stiffnesses ρ_{s1} and ρ_{s2} of the anisotropic Heisenberg model. While the solid circles (black) and squares (red) are the Monte Carlo results of ρ_{s1} and ρ_{s2}, respectively, the up and down triangles are the series expansion results of Ref. 12 for ρ_{s1} and ρ_{s2}, respectively. The solid lines are added to guide the eye.

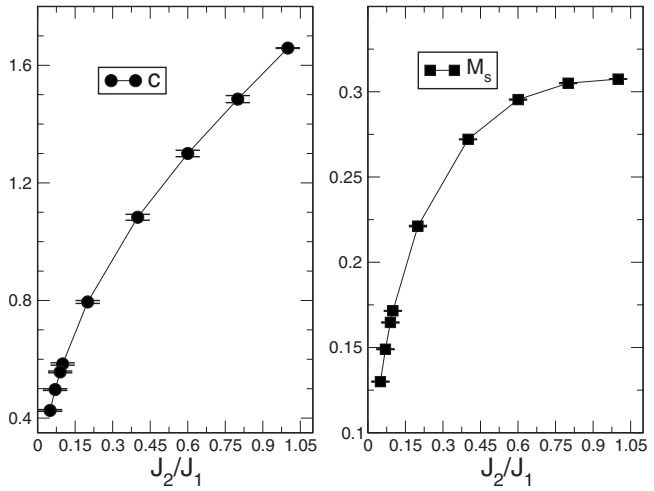

FIG. 4. The J_2/J_1 dependence of the spin wave velocity c (left) and the staggered magnetization density $\mathcal{M}_s$ (right) of the anisotropic Heisenberg model. The solid lines are added to guide the eyes.

esting to consider even stronger anisotropies J_2/J_1 than those used in this study to see how ρ_{s1} approaches its 1D limit. In addition to ρ_{s1} and ρ_{s2}, we have obtained $\mathcal{M}_s$ and c as functions of J_2/J_1 as well from the fits (Fig. 4). The values we obtained for $\mathcal{M}_s$ agree with earlier results in Ref. 6 but have much smaller errors at strong anisotropies.

Next, we would like to turn to discussing the relevance of our results to the pinning effect observed empirically in $YBa_2Cu_3O_{6.45}$. In Ref. 12 it is argued that the J_2/J_1 dependence of the spin stiffnesses in the spatially anisotropic Heisenberg model studied in this work would lead to a very strong pinning energy per Cu site (one order of magnitude larger compared to the corresponding pinning energy in La_2CuO_4). To be more precise, it is the quantity κ that is defined by $\rho_{s2}/\rho_{s1}=1+\kappa(J_2/J_1-1)$ in the weak anisotropy regime that results in the claim made in Ref. 12. Since the spin stiffnesses calculated here agree with those obtained by series expansion in the weak anisotropy regime, which in turn implies that our κ agrees with that in Ref. 12, we conclude that the pinning energy per Cu site is indeed very strong. Hence the in-plane anisotropy of the spin stiffness of the Heisenberg model with anisotropic couplings J_1 and J_2 can indeed provide a possible mechanism for the pinning of the electronic liquid crystal direction in $YBa_2Cu_3O_{6.45}$.

V. CONCLUSIONS

In this note, we have numerically studied the Heisenberg model with anisotropic couplings J_1 and J_2 using a loop cluster algorithm. The corresponding low-energy constants are determined with high precision. Further, the J_2/J_1 dependence of ρ_{s1} and ρ_{s2} is investigated in detail and our results agree quantitatively with those obtained by series expansion[12] in the weakly anisotropic regime. On the other hand, we observe discrepancies between our results and series expansion results in the strongly anisotropic regime. However, the results of our study still lead to very strong pinning energy per Cu site in $YBa_2Cu_3O_{6.45}$, which agrees with the claim made by the authors in Ref. 12. Finally we find that an unexpected behavior of ρ_{s1} might be observed as one approaches much stronger anisotropy regime than those considered in this study.

ACKNOWLEDGMENTS

We would like to thank P. A. Lee, F. Niedermayer, B. C. Tiburzi, and U.-J. Wiese for useful discussions and comments. We would also like to thank T. Pardini, R. R. P. Singh, and O. P. Sushkov for correspondence and providing their series expansion results in Ref. 12. The simulations in this study were performed using the ALPS library, Ref. 22. This work is supported in part by funds provided by the Schweizerischer Nationalfonds (SNF).

*fjjiang@itp.unibe.ch

[1] R. Eder, Y. Ohta, and G. A. Sawatzky, Phys. Rev. B **55**, R3414 (1997).
[2] T. K. Lee and C. T. Shih, Phys. Rev. B **55**, 5983 (1997).
[3] C. J. Hamer, Z. Weihong, and J. Oitmaa, Phys. Rev. B **58**, 15508 (1998).
[4] M. Brunner, F. F. Assaad, and A. Muramatsu, Phys. Rev. B **62**, 15480 (2000).
[5] A. Parola, S. Sorella, and Q. F. Zhong, Phys. Rev. Lett. **71**, 4393 (1993).
[6] A. W. Sandvik, Phys. Rev. Lett. **83**, 3069 (1999).
[7] V. Y. Irkhin and A. A. Katanin, Phys. Rev. B **61**, 6757 (2000).
[8] Y. J. Kim and R. J. Birgeneau, Phys. Rev. B **62**, 6378 (2000).
[9] S. Wenzel, L. Bogacz, and W. Janke, Phys. Rev. Lett. **101**, 127202 (2008).
[10] V. Hinkov, P. Bourges, S. Pailhes, Y. Sidis, A. Ivanov, C. D. Frost, T. G. Perring, C. T. Lin, D. P. Chen, and B. Keimer, Nat. Phys. **3**, 780 (2007).
[11] V. Hinkov *et al.*, Science **319**, 597 (2008).
[12] T. Pardini, R. R. P. Singh, A. Katanin, and O. P. Sushkov, Phys. Rev. B **78**, 024439 (2008).
[13] U.-J. Wiese and H.-P. Ying, Z. Phys. B: Condens. Matter **93**, 147 (1994).
[14] S. Chakravarty, B. I. Halperin, and D. R. Nelson, Phys. Rev. B **39**, 2344 (1989).
[15] H. Neuberger and T. Ziman, Phys. Rev. B **39**, 2608 (1989).
[16] P. Hasenfratz and H. Leutwyler, Nucl. Phys. B **343**, 241 (1990).
[17] P. Hasenfratz and F. Niedermayer, Phys. Lett. B **268**, 231 (1991).
[18] P. Hasenfratz and F. Niedermayer, Z. Phys. B: Condens. Matter **92**, 91 (1993).
[19] S. Eggert, I. Affleck, and M. Takahashi, Phys. Rev. Lett. **73**, 332 (1994).
[20] I. Affleck, M. P. Gelfand, and R. R. P. Singh, J. Phys. A **27**, 7313 (1994).
[21] T. Miyazaki, D. Yoshioka, and M. Ogata, Phys. Rev. B **51**, 2966 (1995).
[22] A. F. Albuquerque *et al.*, J. Magn. Magn. Mater. **310**, 1187 (2007).